EUROPEAN ORGANIZATION FOR NUCLEAR RESEARCH

CERN-EP/83-80
16 June 1983

PHOTOPRODUCTION OF $K\bar{K}\pi$ FINAL STATES IN THE PHOTON ENERGY RANGE FROM 20 TO 70 GeV

The OMEGA Photon Collaboration

Bonn[1]-CERN[2]-Glasgow[3]-Lancaster[4]-Manchester[5]-Paris VI[6]-Rutherford[7]-Sheffield[8]

M. Atkinson[7], T.J. Axon[5], D. Barberis[5], T.J. Brodbeck[4], G.R. Brookes[8], J.J. Bunn[8], P.J. Bussey[3], A.B. Clegg[4], J.B. Dainton[3], M. Davenport[7], B. Dickinson[5], B. Diekmann[1], A. Donnachie[5], R.J. Ellison[5], P. Flower[7], P.J. Flynn[4], W. Galbraith[5], K. Heinloth[1], R.C.W. Henderson[4], R.E. Hughes-Jones[5], J.S. Hutton[7], M. Ibbotson[5], H.P. Jakob[1], M. Jung[1], M.A.R. Kemp[7], B.R. Kumar[7], J. Laberrigue[6], G.D. Lafferty[5], J.B. Lane[5], J.C. Lassalle[2], J.M. Levy[6], V. Liebenau[1], R.H. McClatchey[8], D. Mercer[5], J.A.G. Morris[7], J.V. Morris[7], D. Newton[4], C. Paterson[3], G.N. Patrick[2], E. Paul[1], C. Raine[3], M. Reidenbach[1], H. Rotscheidt[1], A. Schlösser[1], P.H. Sharp[7], I.O. Skillicorn[3], K.M. Smith[3], K.M. Storr[2], R.J. Thompson[5], Ch. de la Vaissière[6], A.P. Waite[5] and T.P. Yiou[6]

ABSTRACT

The reactions $\gamma p \to K^+K^-\pi^0(p)$ and $\gamma p \to K^0_S K^{\pm}\pi^{\mp}(p)$ have been measured using tagged photons in the energy range 20 to 70 GeV. No resonance structure is observed in either of the $K\bar{K}\pi$ invariant mass distributions, which range from threshold up to $\sim$ 3 GeV. The photoproduction cross-sections for $\phi\pi^0$ and $K^*(892)K$ are presented and are compared with theoretical predictions. No evidence has been found for the photoproduction of $\phi'(1680)$.

(To be submitted to Nuclear Physics B)

1. INTRODUCTION

We report on the measurement of 359 events of the reaction

$$\gamma p \to K^+K^-\pi^0(p) \tag{1}$$

and 265 events of the reaction

$$\gamma p \to K^0_S K^{\pm}\pi^{\mp}(p) \quad \Big\lfloor \to \pi^+\pi^- \tag{2}$$

with tagged photons of energy E_γ in the range 20 to 70 GeV. This experiment covers the $K\bar{K}\pi$ invariant mass range up to about 3 GeV. No measurements of these high-energy photoproduction processes have previously been made.

In the e^+e^- annihilation reaction

$$e^+e^- \to K^0_S K^{\pm}\pi^{\mp} \tag{3}$$

an enhancement has been reported at 1.68 GeV with a width of $\sim$ 185 MeV decaying dominantly via $K^*(892)K^0_S$, which is interpreted to be mainly due to a radial excitation of the $\phi(1020)$ [1]. This $\phi'(1680)$ state should be produced in the photoproduction reactions (1) and (2). The photoproduction cross-section can be estimated from the e^+e^- annihilation cross-section using simple vector meson dominance (VDM). In addition, states with J^P other than 1^- may also contribute in diffractive photoproduction.

Isospin relations for the production of an isoscalar state decaying via $K^*(892)K$ give the following ratio for the cross-sections

$$\frac{\sigma(\gamma p \to K^*Kp \to K^0K^{\pm}\pi^{\mp}\, p)}{\sigma(\gamma p \to K^*Kp \to K^+K^-\pi^0 p)} = 4 \ .$$

(This ratio is the same for an isovector state.)

2. EXPERIMENTAL SET-UP AND DATA REDUCTION

The experiment used an 80(±2%) GeV electron beam to produce tagged photons of energies 20-70 GeV. The particles resulting from interaction of these photons in a 60 cm liquid-hydrogen target were detected in the Omega spectrometer, equipped

with multiwire proportional chambers (MWPCs), drift chambers, a threshold gas Čerenkov counter and a large-aperture photon detector [2]. The trigger requirements were:

i) a signal from the photon tagging logic;

ii) a signal to indicate an interaction in the hydrogen target producing at least two forward charged particles;

iii) in order to suppress electromagnetic background, either no signal from a shower counter array in the median plane downstream of the magnet, or else a hit in a MWPC inside the Omega spectrometer well away from this median plane;

iv) for reaction (1) a signal from the high-resolution photon detector, and for reaction (2) a signal from an on-line logic (K-matrix) to indicate the presence of at least one charged track giving no light in the Čerenkov counter [3].

In the data reduction, events were selected as follows:

i) The tagged photon must have been unambiguously measured, i.e. the incident and scattered electron must have been reconstructed in the tagging system.

ii) Two or three charged particles were required to be reconstructed to a main vertex, within the hydrogen target, with a net charge of 0 or 1 (in the latter case the third charged track had to be consistent with the hypothesis of a recoil proton).

iii) For reaction (1) both fast particles had to be consistent with a K^+K^-, i.e. they must have had momenta between 5 GeV/c (π threshold) and 17 GeV/c (kaon threshold) and must have given no light in the Čerenkov counter. For reaction (2) one track had to be consistent with $K^{\pm}$ and the other with $\pi^{\mp}$.

iv) A well-reconstructed π^0 from the photon detector was required for reaction (1) and a well-reconstructed K^0_S decaying into $\pi^+\pi^-$ for reaction (2).

Figures 1a and b show the distribution of the missing energy $\Delta E = E_\gamma - E_{K\bar{K}\pi} - T_p$ (T_p is the kinetic energy of the proton and is included when measured) for reactions (1) and (2), respectively. The final selection of reactions (1) and (2) required $|\Delta E|$ to be less than 1.5 GeV. The remaining data samples consisted of 359 events for reaction (1) and 265 events for reaction (2). We estimate that the inelastic contamination is $\sim$ 20% for reaction (1) and $\sim$ 15% for reaction (2).

Any background from the process $\gamma p \to \pi^+\pi^-\pi^0(p)$ in reaction (1) is found to be negligible, as is shown by the absence of an $\omega(783)$ peak in fig. 2. This figure shows the invariant mass $m_{\pi^+\pi^-\pi^0}$ of events from reaction (1) with the $\pi^\pm$ mass assigned to the charged kaons. Background from the reaction $\gamma p \to p\bar{p}\pi^0(p)$ in reaction (1) is found to be small by measuring the number of events of this type in the momentum range where the Čerenkov counter is able to distinguish between protons and kaons ($17 < p_{p,\bar{p}} < 33$ GeV/). We found 4 events of this reaction.

A contamination of our $K^0_S \to \pi^+\pi^-$ sample in reaction (2) by misidentified e^+e^- pairs or $\Lambda,\bar{\Lambda}$ is also found to be negligible. The invariant mass of the $\pi^+\pi^-$ system from the V^0 decay indicates a clear K^0_S signal with little background.

3. EXPERIMENTAL ACCEPTANCE

The acceptance of the apparatus was calculated by Monte Carlo simulations with the following input:

i) E_γ spectrum as measured by a subsidiary monitor trigger, which merely required a signal from an end-cap scintillation counter immediately following the hydrogen target;

ii) cross-section independent of E_γ (see fig. 3) and falling with four-momentum transfer squared t from the photon to the $K\bar{K}\pi$ system as exp (-4t) for both reactions (1) and (2);

iii) a flat decay angular distribution W(cos θ) where θ is defined as the angle between the normal to the ($K\bar{K}\pi$) decay plane in the $K\bar{K}\pi$ rest frame and the s-channel helicity axis;

iv) an invariant $K\bar{K}\pi$ mass distribution similar to our experimental $K\bar{K}\pi$ distribution (see fig. 6);

v) the same fraction of resonant $K^*(892) \rightarrow K\pi$ subsystems as found in our data (see section 4).

These generated events were now passed through a program chain which simulated the experimental conditions, including:

i) geometrical trigger acceptance of the spectrometer for each trigger discussed above;

ii) track reconstruction and vertex fitting efficiency including a full simulation of the V^0 reconstruction;

iii) charged and neutral particle identification efficiencies, in particular a full simulation of showering in the photon detector.

The general features of the data are well reproduced by this simulation. For example in figs. 3a and b we show the distribution of E_γ for reactions (1) and (2) compared with the simulation. These are consistent with a constant or only slowly falling cross-section as a function of E_γ for both reactions. Figures 4a and b show the comparison for the K^0_S decay length and distance to main vertex. The good agreement demonstrates that the K^0_S acceptance is well understood.

4. EXPERIMENTAL RESULTS

Figure 5a shows the K^+K^- mass spectrum from reaction (1); about 7% of these events can be assigned to $\phi\pi^0$ production ($1.01 < m_{K^+K^-} < 1.03$ GeV/c^2), corresponding to a cross-section $\sigma(\gamma p \rightarrow \phi\pi^0 p)$ of 6 ± 3 nb (see section 5). The corresponding mass spectrum is shown in fig. 5b. It has been suggested that diffractive photoproduction of $\phi\pi^0$ could be a signature for production of four-quark states with a predicted cross-section of at least 100 nb [4], considerably in excess of what we observe. We exclude this subsample of reaction (1) from further analysis, leaving 332 events.

Figures 6a and b show the $K\bar{K}\pi$ mass spectra for reactions (1) and (2). No evidence for narrow resonance structure is seen in either of these distributions. The mass resolution in both final states is calculated to be 60 MeV (FWHM). The invariant mass spectra of the $K\pi$ substates for reactions (1) and (2) are shown in figs. 7a to d and indicate substantial $K^*(892)$ production. Fits to these distributions give K^* masses and widths in good agreement with their nominal values. We find the following fractions of K^* production: for reaction (1), $(16 \pm 3)\%$ K^{*+}, $(13 \pm 3)\%$ K^{*-}; and for reaction (2), $(16 \pm 4)\%$ K^{*0}, $(19 \pm 4)\%$ $K^{*\pm}$.

Figure 8a shows the $K^+K^-\pi^0$ mass distribution from reaction (1) for those events where a $K\pi$ substate lies in the K^* mass range ($0.83 < m_{K\pi} < 0.96$ GeV/c^2). Figure 8b corresponds to those events where a $K\pi$ system lies in the K^* mass wings ($0.77 < m_{K\pi} < 0.83$ or $0.96 < m_{K\pi} < 1.02$ GeV/c^2). Figures 8c and d are the corresponding plots for reaction (2). No evidence for resonant-like structure is seen in these K^*K invariant mass distributions.

Figures 9a and b show the four-momentum transfer squared distributions, corrected for acceptance losses, for reactions (1) and (2), respectively. The solid line corresponds to a fit in the range $0.05 < t < 0.8$ $(\text{GeV}/c)^2$ of the form $d\sigma/dt = A \exp(-bt)$, giving the slope parameters $b = (4.0 + 0.4)$ $(\text{GeV}/c)^{-2}$ for both reactions (1) and (2).

In figs. 10a and c $\cos\theta$ (where θ is defined as in section 3) is plotted for reactions (1) and (2), respectively. Figures 10b and d show the same distributions for the subsample of reactions (1) and (2), for which the $K\pi$ system lies within the K^* mass range. These four distributions are also corrected for acceptance losses. For diffractive photoproduction of a $J^P = 1^-$ state, assuming s-channel helicity conservation (SCHC), one expects a decay angular distribution $W(\cos\theta) \propto \sin^2\theta$. We have fitted the expression $W(\cos\theta) = A(1 + B \sin^2\theta)$ to the distributions in figs. 10a and c and find values of B of 0.0 ± 0.1 for reaction (1) and $0.4 + 0.1$ for reaction (2). We conclude that the production by an SCHC mechanism of $J^P = 1^-$ does not dominate the data; this holds also for the K^*K subsystems (see figs. 10b and d).

5. CROSS-SECTIONS

For the reactions (1) and (2), after subtraction of the inelastic contamination and averaging over the photon energy range 20 to 70 GeV, we find the following cross-sections:

$$\sigma(\gamma p \to K^+K^-\pi^0 p) = 80 \pm 5 \pm 20 \text{ nb}$$

$$\sigma(\gamma p \to K^0_S K^\pm \pi^\mp p) = 102 \pm 9 \pm 44 \text{ nb}$$

(corrected for the undetected decay modes of K^0_S). The errors quoted are statistical and systematic, respectively. Taking the fractions of resonant $K^*(892)$ production measured in these reactions, we obtain for the $K^*(892)K$ cross-sections:

$$\sigma(\gamma p \to K^{*+}K^- p \to K^+\pi^0 K^- p) = 13 \pm 3 \pm 4 \text{ nb}$$

$$\sigma(\gamma p \to K^{*-}K^+ p \to K^-\pi^0 K^+ p) = 10 \pm 3 \pm 4 \text{ nb}$$

$$\sigma(\gamma p \to K^{*0}K^0_S p \to K^\pm\pi^\mp K^0_S p) = 16 \pm 4 \pm 8 \text{ nb}$$

$$\sigma(\gamma p \to K^{*\pm}K^\mp p \to K^0_S\pi^\pm K^\mp p) = 19 \pm 4 \pm 8 \text{ nb} .$$

The ratio of cross-sections discussed in section 1 is measured to be 3.0 ± 0.6 (using statistical errors only, taking into account that K^0_S represents $\frac{1}{2}$ of the total K^0 production).

6. COMPARISON WITH e^+e^- ANNIHILATION

In order to compare our results with the recent observation [1] of a $\phi'(1680)$ candidate in the e^+e^- annihilation reaction (3), we assume the simple VDM relation (which has been calibrated for $\rho'(1600)$ photoproduction [5])

$$\sigma_{peak}(e^+e^- \to \phi') = \frac{64\pi^2\alpha b}{m_{\phi'}\Gamma_{\phi'}} \frac{\sigma(\gamma p \to \phi' p)}{\sigma^2_{tot}(\phi' p)} .$$

Using the values

$$\sigma_{peak}(e^+e^- \to \phi') = 5 \text{ nb}$$

$$m_{\phi'} = 1.68 \text{ GeV}$$

$$\Gamma_{\phi'} = 185 \text{ MeV}$$

$$b = 4 \text{ GeV/c}$$

$$\sigma_{tot}(\phi' p) = 9 \text{ mb}$$

we obtain $\sigma(\gamma p \to \phi' p) \approx 45$ nb. This is about 40% of our total measured $K^0_S K^{\pm}\pi^{\mp}$ cross-section. Figure 11a shows the comparison of our acceptance-corrected $K^0_S K^{\pm}\pi^{\mp}$ mass spectrum with the predicted signal from e^+e^-. Our result is clearly incompatible with a narrow peak of this magnitude at 1.68 GeV. Figures 11b and c show the mass spectra for $K^{*\pm}$ and K^{*0} selected events (i.e. $K\pi$ mass in the range 0.83-0.96 GeV/c with no background subtraction). Neither of these distributions show a narrow peak, in particular the K^{*0} selected distribution is inconsistent with the observation of a ϕ' signal in $e^+e^- \to K^{*0}K^0_S$, as is shown by the curve in fig. 11c. Using fig. 11c, we calculate an upper limit of 5 nb (90% CL) for the photoproduction cross-section in $K^{*0}K^0_S$. In order to resolve this inconsistency between e^+e^- annihilation and photoproduction one would need either a serious breakdown of the simple VDM relation above, in disagreement with findings in $\rho'(1600)$ photoproduction [5], or else complicated interference effects such as between $\phi'(1680)$ and $\rho'(1600)$ (which decays also into K^*K [1]) contributing with different relative amplitudes to e^+e^- annihilation and photoproduction. The parametrization of interference effects in photoproduction would not be straightforward, so that any conclusion would be strongly model-dependent.

7. CONCLUSIONS

We have measured the elastic photoproduction of $K^+K^-\pi^0$ and $K^0_S K^{\pm}\pi^{\mp}$ over the incident photon energy range 20-70 GeV. We find cross-sections of 80 ± 5 ± 20 nb for $K^+K^-\pi^0$ (excluding $\phi\pi^0$) and 102 ± 9 ± 44 nb for $K^0_S K^{\pm}\pi^{\mp}$. The cross-section for $\phi\pi^0$ production is 6 ± 3 nb, an order of magnitude lower than that predicted for diffractive photoproduction of four-quark states. There is substantial $K^*(892)$ production corresponding to 29 ± 5% $K^{*\pm}$ for the first reaction and 35 ± 6% $K^{*\pm}$ for the second reaction, the ratio of these being consistent with isospin predictions. No evidence for $K\bar{K}\pi$ resonance production has been found in any of these channels studied. In particular, no evidence has been found for the photoproduction of $\phi'(1680)$ decaying via $K^*(892)K^0_S$.

Acknowledgements

We are grateful to the Omega group at CERN for their help in running the spectrometer and providing on-line and off-line software. The work of the technical support staff in our home institutions, and the support at the computer centres at the Rutherford Appleton Laboratory, CERN, and the RHRZ at Bonn have been invaluable. We thank the SERC (UK), the BMFT (Fed. Rep. Germany), and the IN2P3 (France) for financial support.

* * *

REFERENCES

[1] J. Buon et al., Phys. Lett. 118B (1982) 221.

[2] D. Aston et al., Nucl. Instrum. Methods 197 (1982) 287.
Experiments at CERN in 1980 (CERN, Geneva, 1980).

[3] T. Armstrong et al., Nucl. Instrum. Methods 175 (1980) 543.

[4] F.E. Close, Phys. Rev. 41 (1978) 1263.

[5] D. Aston et al., Nucl. Phys. 189B (1981) 15.

Figure captions

Fig. 1 : a) Distribution of missing energy for reaction (1) (see text); the solid line represents a hand-drawn background curve.

b) Distribution of missing energy for reaction (2) (see text); the solid line represents a hand-drawn background curve.

Fig. 2 : Invariant mass $m_{\pi^+\pi^-\pi^0}$ for events of reaction (1) assigning the pion mass to the charged kaons.

Fig. 3 : a) Distribution of E_γ for reaction (1); the solid line corresponds to simulated events.

b) Distribution of E_γ for reaction (2); the solid line corresponds to simulated events.

Fig. 4 : a) K^0_S decay length from reaction (2); the solid line corresponds to simulated events.

b) Distribution of distance to main vertex for K^0_S from reaction (2), the solid line corresponds to simulated events.

Fig. 5 : a) Invariant mass of K^+K^- for events of reaction (1). The dashed line corresponds to the geometrical acceptance.

b) Invariant mass of $K^+K^-\pi^0$ for events of reaction (1), where $1.01 < m_{K^+K^-} < 1.03$ GeV/c^2. The dashed line corresponds to the geometrical acceptance.

Fig. 6 : a) Invariant mass of $K^+K^-\pi^0$ for events of reaction (1). The dashed line corresponds to the geometrical acceptance.

b) Invariant mass of $K^0_S K^\pm \pi^\mp$ for events of reaction (2). The dashed line corresponds to the geometrical acceptance.

Fig. 7 : Distributions of the invariant mass $m_{K\pi}$. Solid line corresponds to a fit assuming a Breit-Wigner resonance profile for $K^*(892) \to K\pi$ and an exponential background. Dashed line represents the geometrical acceptance a) for $K^+\pi^0$ combination from reaction (1); b) for $K^-\pi^0$ combinations from reaction (1); c) for $K^\pm\pi^\mp$ combinations from reaction (2); d) for $K^0_S\pi^\pm$ combinations from reaction (2).

Fig. 8 : a) Invariant mass of $K\bar{K}\pi$ for reaction (1) where $0.83 < m_{K\pi} < 0.96$ GeV/c^2. The dashed line corresponds to geometrical acceptance.

b) Invariant mass of $K\bar{K}\pi$ for reaction (1) where $0.77 < m_{K\pi} < 0.83$ or $0.96 < m_{K\pi} < 1.02$ GeV/c^2. The dashed line corresponds to geometrical acceptance.

c) Invariant mass of $K\bar{K}\pi$ for reaction (2) where $0.83 < m_{K\pi} < 0.96$ GeV/c^2. The dashed line corresponds to geometrical acceptance.

d) Invariant mass of $K\bar{K}\pi$ for reaction (2) where $0.77 < m_{K\pi} < 0.83$ or $0.96 < m_{K\pi} < 1.02$ GeV/c^2. The dashed line corresponds to geometrical acceptance.

Fig. 9 : a) Distribution of four-momentum transfer squared t for reaction (1) corrected for acceptance. The solid line corresponds to a fit as described in the text.

b) Distribution of four-momentum transfer squared t for reaction (2) corrected for acceptance. The solid line corresponds to a fit as described in the text.

Fig. 10 : a) Decay angular distribution cos θ for events of reaction (1) corrected for acceptance.

b) Decay angular distribution cos θ for events of reaction (1) corrected for acceptance where the Kπ invariant mass lies within the $K^*(892)$ mass range ($0.83 < m_{K\pi} < 0.96$ GeV/c).

c) Decay angular distribution cos θ for events of reaction (2) corrected for acceptance.

Fig. 10 : d) Decay angular distribution cos θ for events of reaction (2) corrected for acceptance where the $K\pi$ invariant mass lies within the $K^*(892)$ mass range ($0.83 < m_{K\pi} < 0.96$ GeV/c).

Fig. 11 : a) $d\sigma/dm$ for $K^0_S K^{\pm}\pi^{\mp}$. Solid curve is the VDM expectation from the e^+e^- annihilation as described in the text.

b) $d\sigma/dm$ for $K^0_S K^{\pm}\pi^{\mp}$ where the $K^0\pi^{\pm}$ combination lies within the $K^*(892)$ mass range.

c) $d\sigma/dm$ for $K^0_S K^{\pm}\pi^{\mp}$ where the $K^{\pm}\pi^{\mp}$ combination lies within the $K^*(892)$ mass range. The solid curve is described in the text.

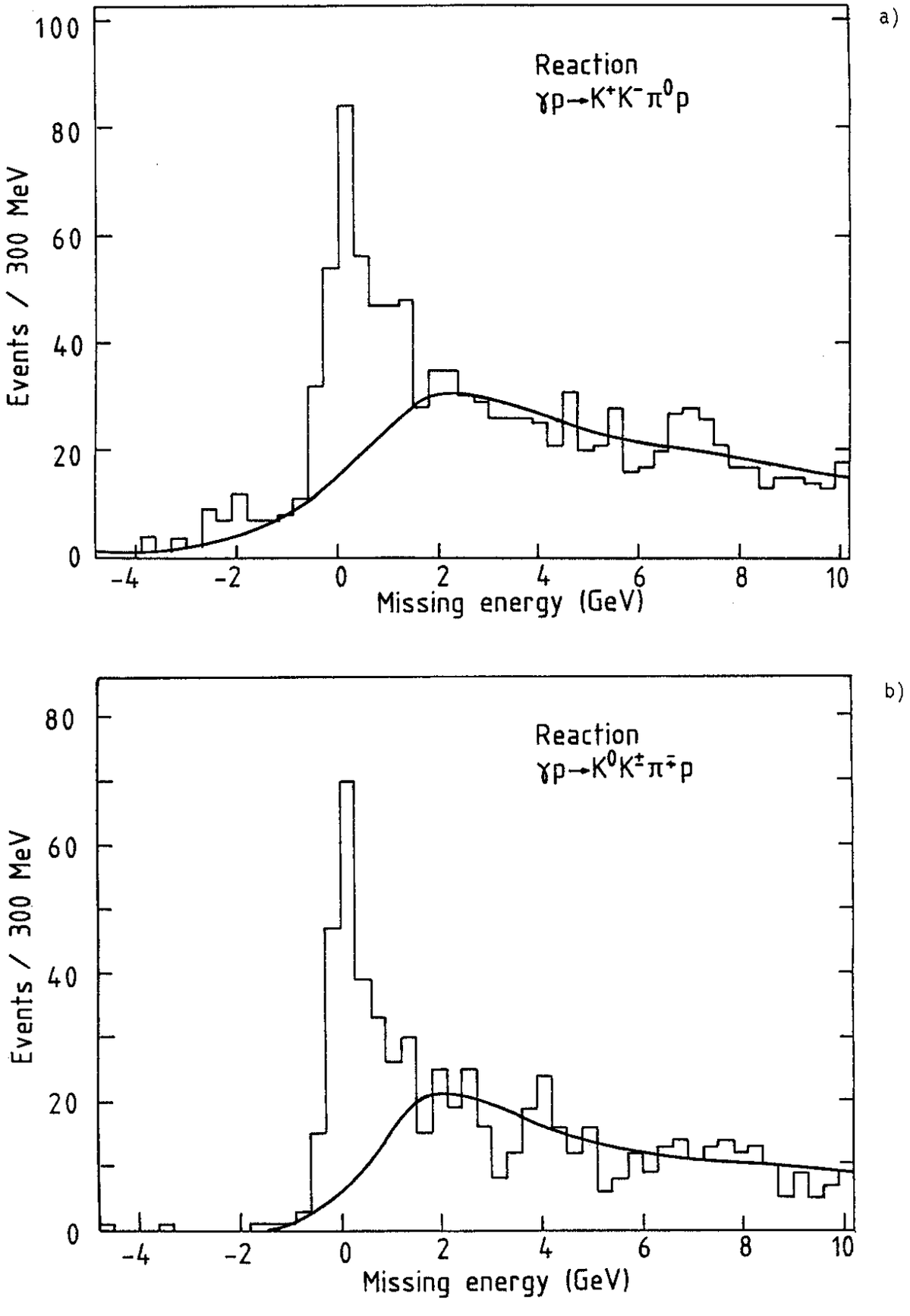
a)
Reaction
γp→K⁺K⁻π⁰p
Events / 300 MeV
Missing energy (GeV)
b)
Reaction
γp→K⁰K±π∓p
Events / 300 MeV
Missing energy (GeV)

Fig. 1

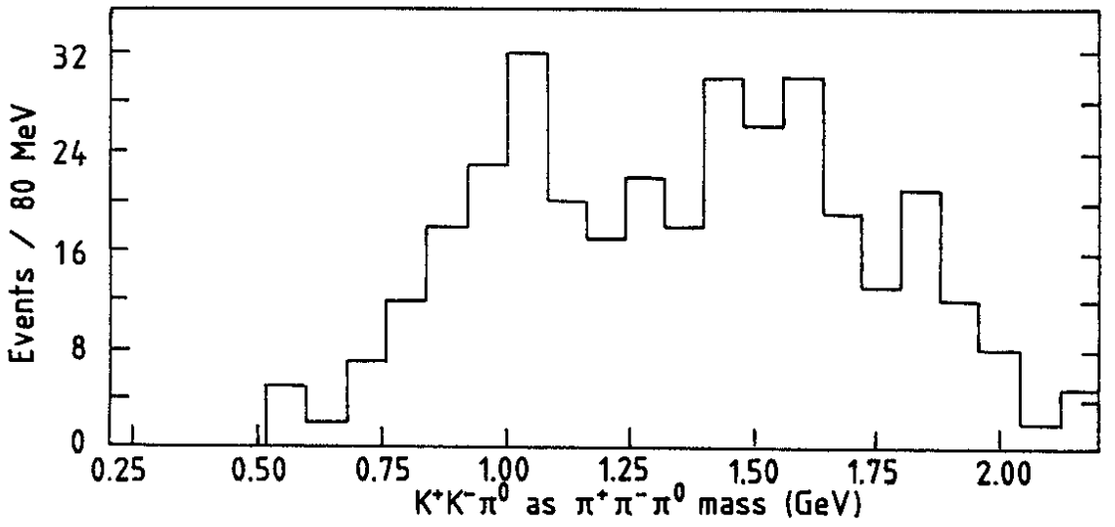

Fig. 2

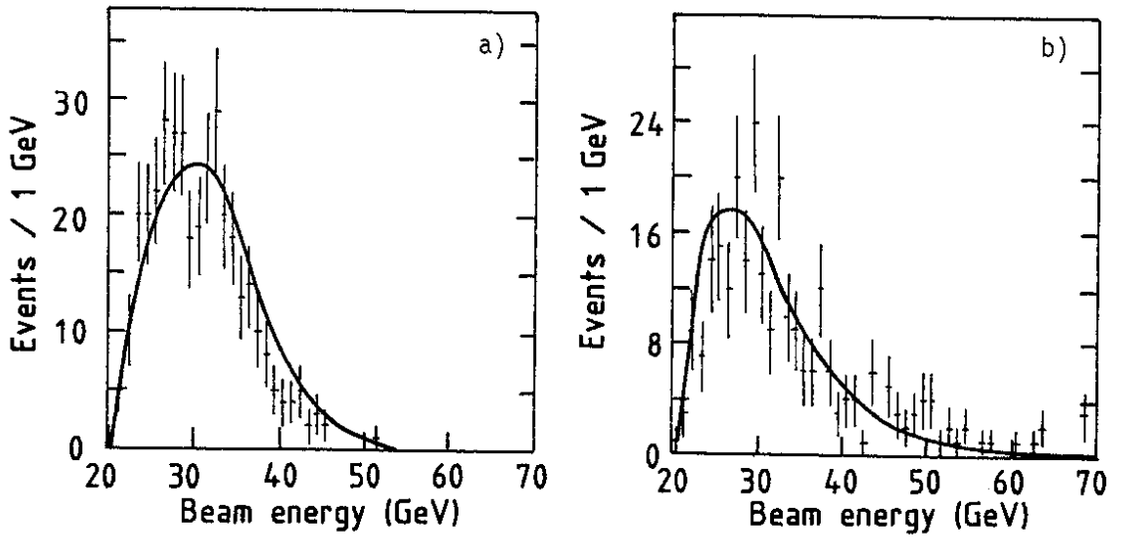

Fig. 3

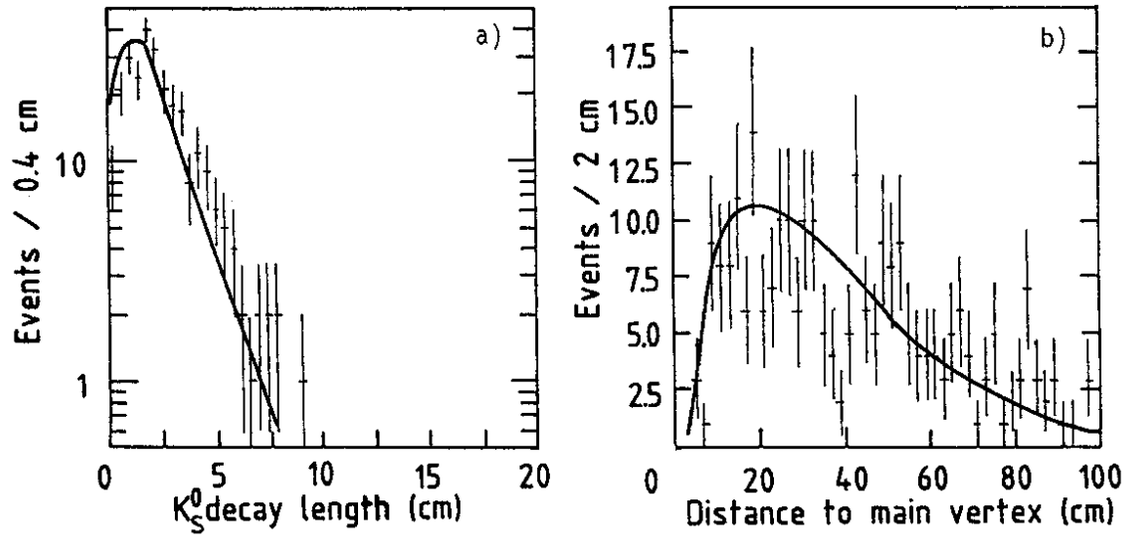

Fig. 4

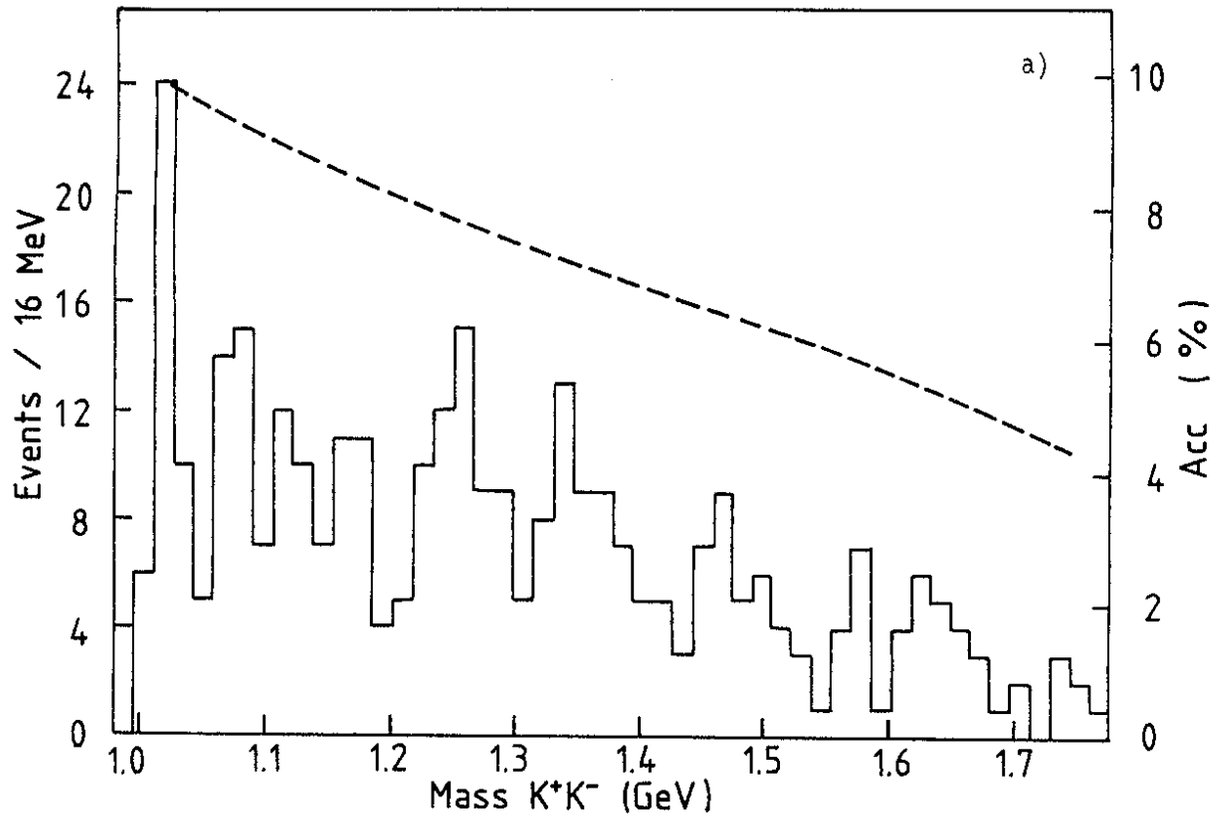
a)
Events / 16 MeV
Acc (%)
Mass K⁺K⁻ (GeV)
0
4
8
12
16
20
24
2
6
10
1.0
1.1
1.2
1.3
1.4
1.5
1.6
1.7

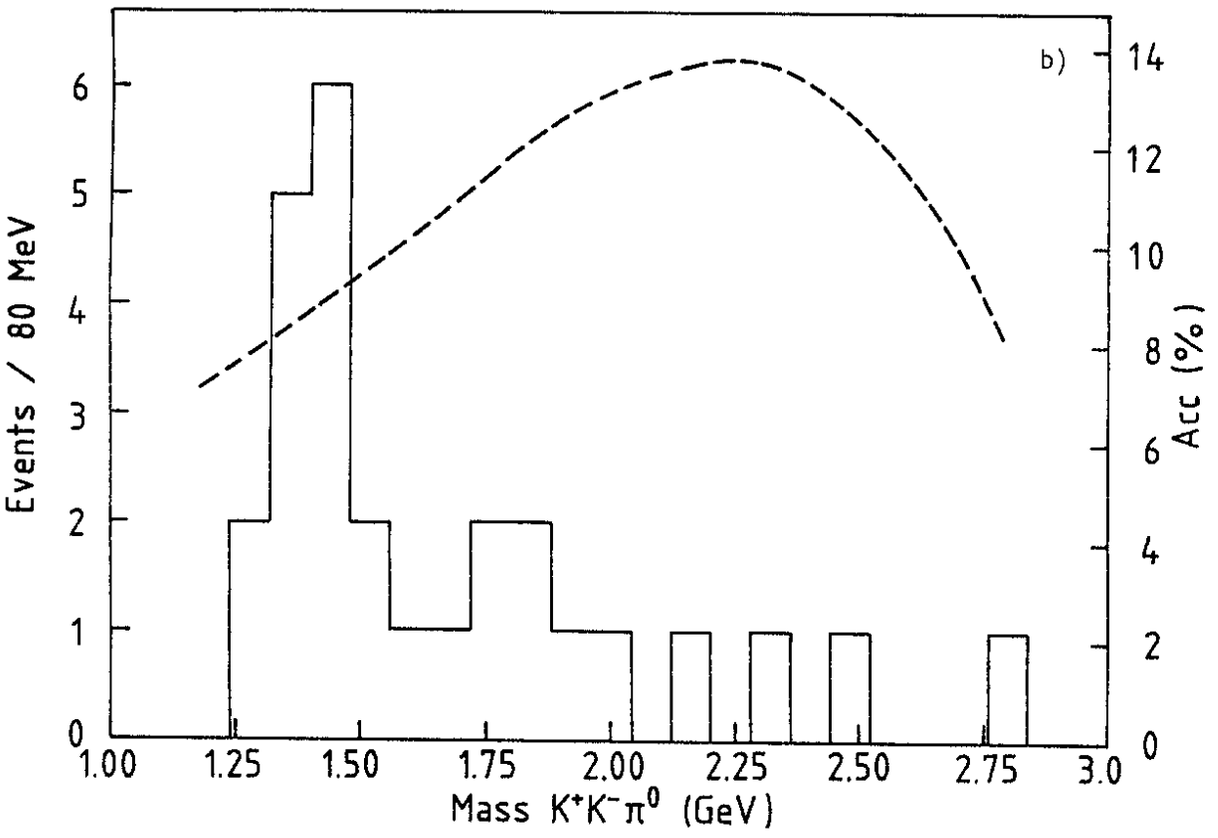
b)
Events / 80 MeV
Acc (%)
Mass K⁺K⁻π⁰ (GeV)
0
1
2
3
4
5
6
8
10
12
14
1.00
1.25
1.50
1.75
2.00
2.25
2.50
2.75
3.0

Fig. 5

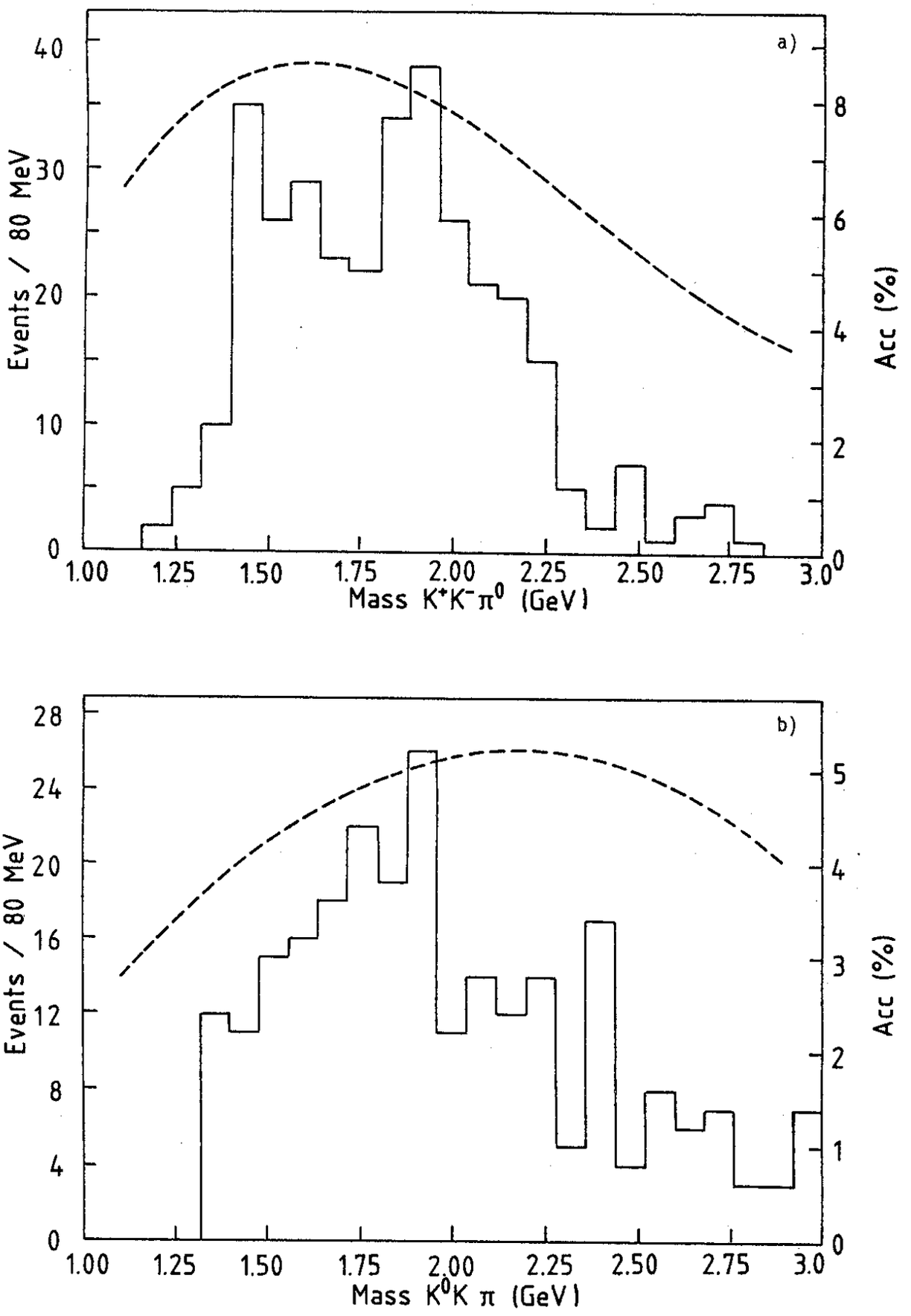
a)
Events / 80 MeV
Acc (%)
Mass $K^+K^-\pi^0$ (GeV)
b)
Events / 80 MeV
Acc (%)
Mass $K^0K\pi$ (GeV)

Fig. 6

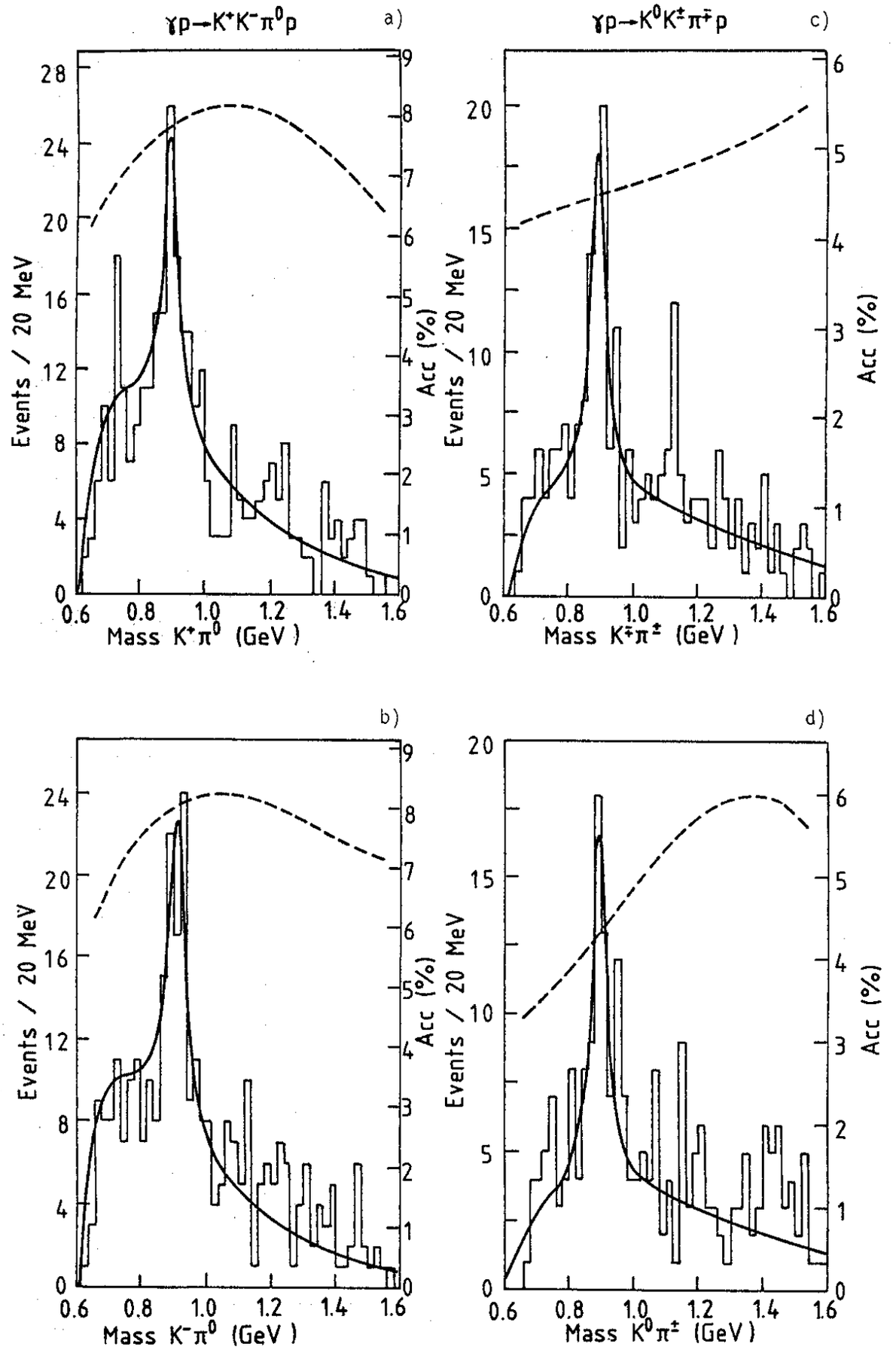
γp→K⁺K⁻π⁰p
a)
γp→K⁰K±π∓p
c)
Events / 20 MeV
Acc (%)
Mass K⁺π⁰ (GeV)
Mass K±π∓ (GeV)
b)
d)
Mass K⁻π⁰ (GeV)
Mass K⁰π± (GeV)

Fig. 7

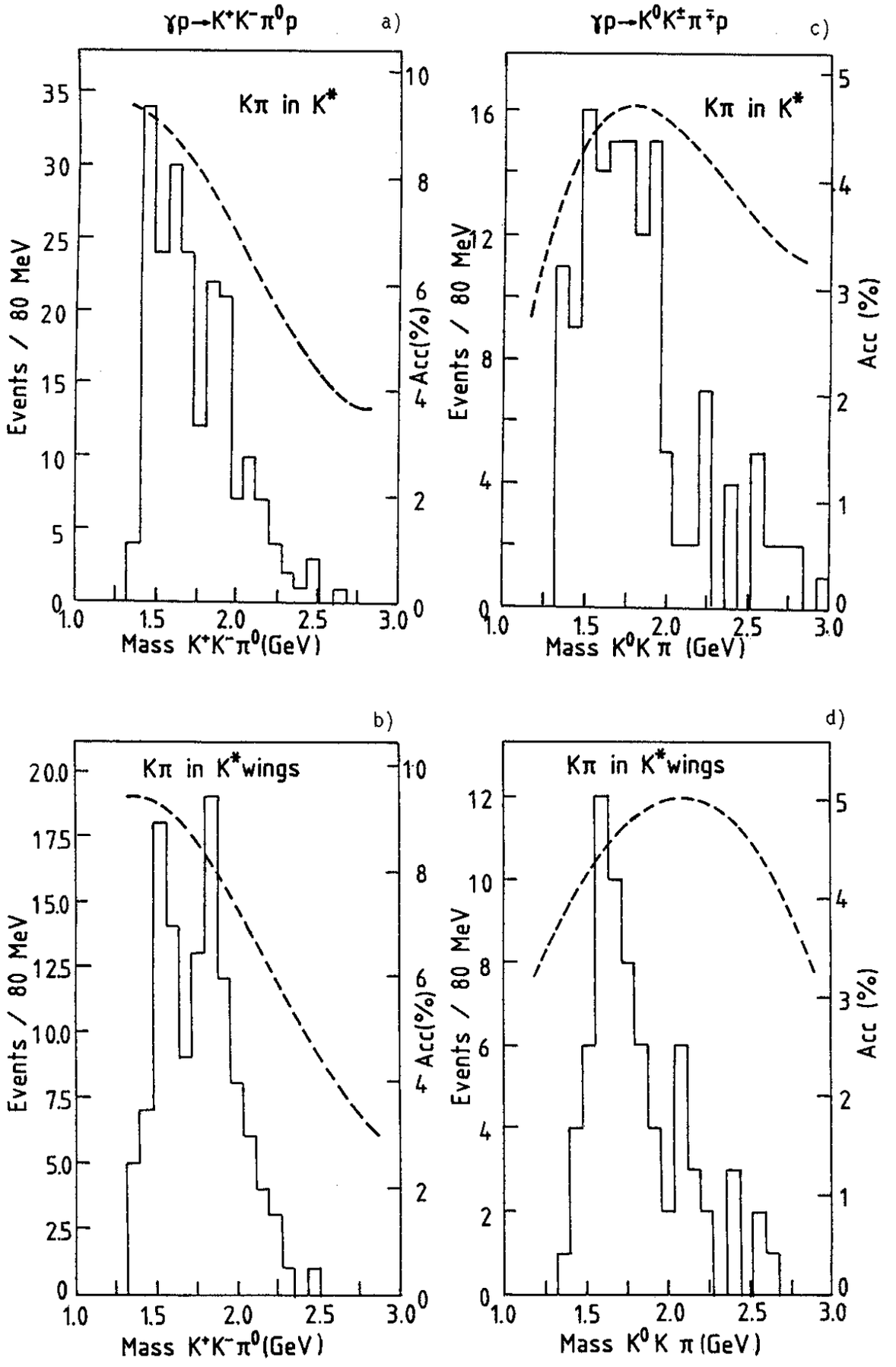
γp→K⁺K⁻π⁰p
a)
Kπ in K*
Events / 80 MeV
Acc(%)
Mass K⁺K⁻π⁰(GeV)
γp→K⁰K±π∓p
c)
Kπ in K*
Events / 80 MeV
Acc (%)
Mass K⁰K π (GeV)
b)
Kπ in K*wings
Events / 80 MeV
Acc(%)
Mass K⁺K⁻π⁰(GeV)
d)
Kπ in K*wings
Events / 80 MeV
Acc (%)
Mass K⁰K π (GeV)

Fig. 8

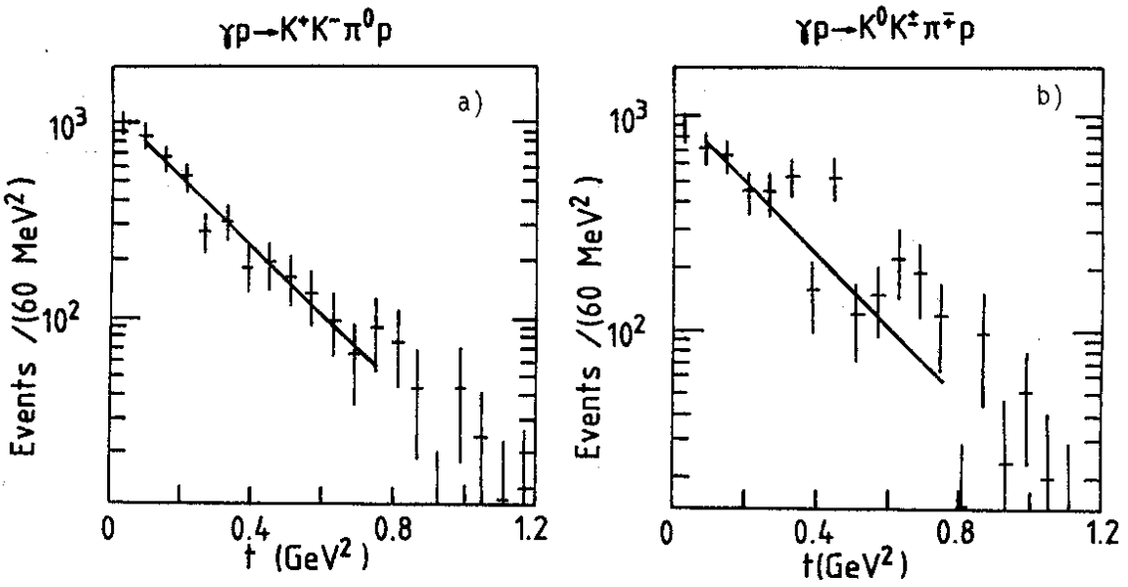
γp→K⁺K⁻π⁰p
γp→K⁰K±π∓p
a)
b)
Events /(60 MeV²)
t (GeV²)
t(GeV²)

Fig. 9

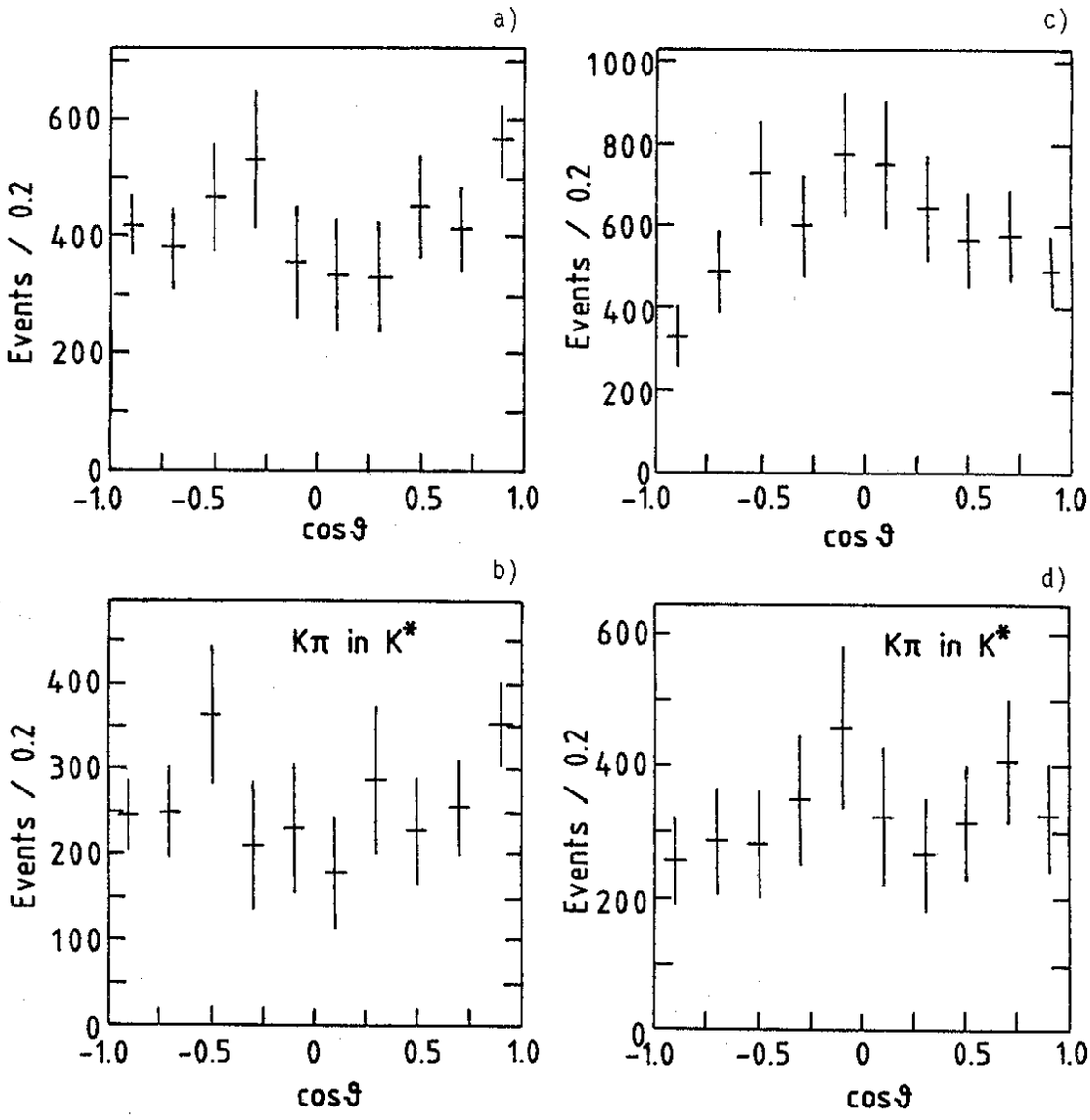
a)
b)
c)
d)
Events / 0.2
cos ϑ
Kπ in K*

Fig. 10

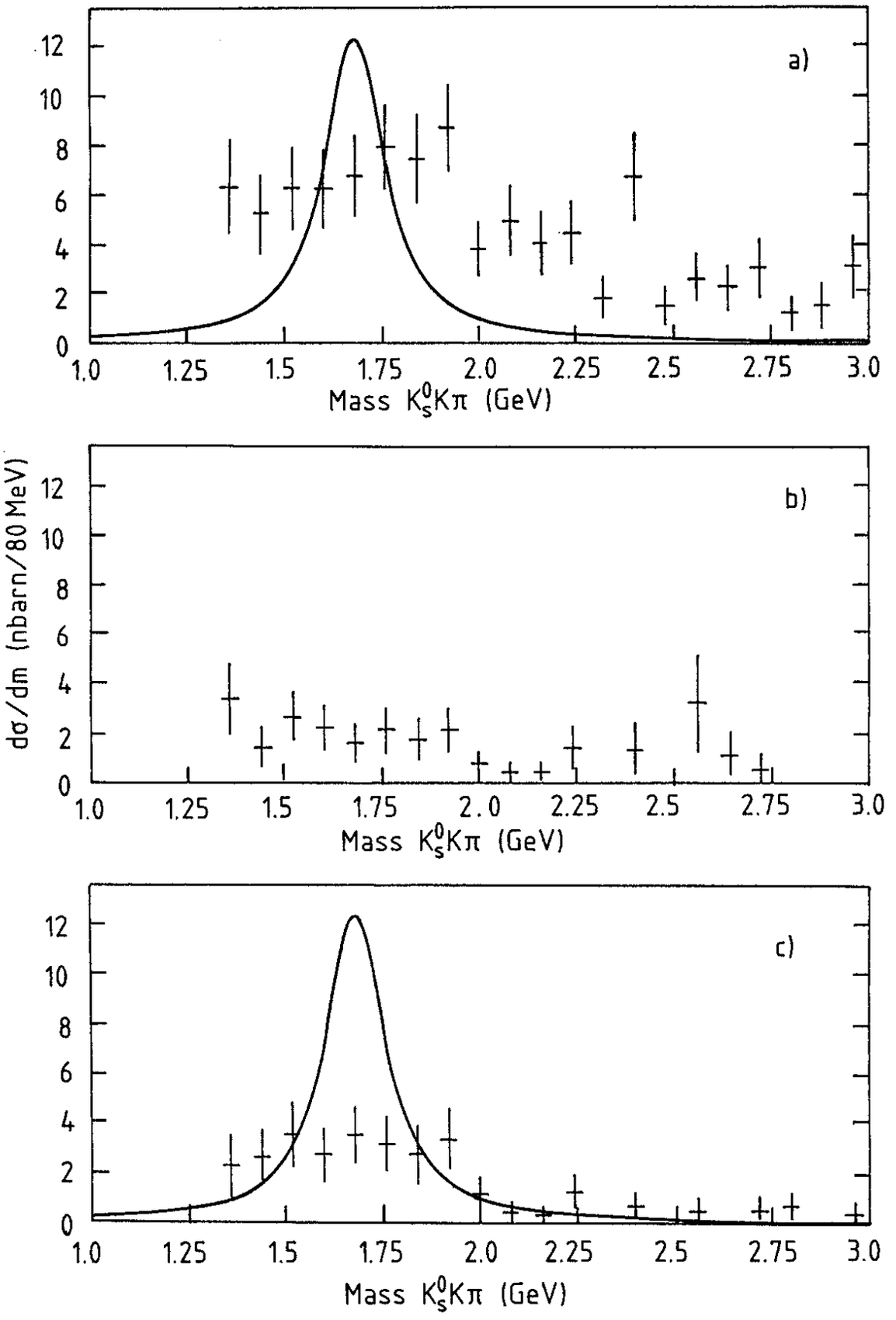
a)
b)
c)
dσ/dm (nbarn/80 MeV)
Mass $K^0_s K\pi$ (GeV)
1.0
1.25
1.5
1.75
2.0
2.25
2.5
2.75
3.0
0
2
4
6
8
10
12

Fig. 11